17-825.R1 Poulsom EDITED USA English ORIGINAL PAPER

PLEASE NOTE REVISED TITLE HERE IS AGREED WITH AUTHORS

Activation of MET signaling by HDAC6 offers a rationale for a novel ricolinostat and crizotinib combinatorial therapeutic strategy in diffuse large B-cell lymphoma

Zebing Liu[1,2†], Ying Cai[1,3†], Yu Yang[4†], Anqi Li[1], Rui Bi[1], Lisha Wang[5], Xiaohan Shen[1], Weige Wang[1], Yijun Jia[1], Baohua Yu[1], Bing Cao[1], Wenli Cui[1], Ping Wei[1], Xiaoyan Zhou[1,6*]

[1] Department of Pathology, Fudan University Shanghai Cancer Center; Department of Oncology, Shanghai Medical College, Fudan University, Shanghai 200032, China

[2] Department of Pathology, Renji Hospital, School of Medicine, Shanghai Jiao Tong University, Shanghai 200127, China

[3] Department of Pathology, Wuxi People's Hospital Affiliated to Nanjing Medical University, Wuxi 214023, Jiangsu, China

[4] Scientific Research Center, Shanghai Public Health Clinical Center, Fudan University, Shanghai 201508, China

[5] Michigan Center for Translational Pathology, University of Michigan Medical School, Ann Arbor 48109, MI, USA

[6] Institute of Pathology, Fudan University, Shanghai 200032, China

[†] Equal contributions.

*Correspondence to: Xiaoyan Zhou, Department of Pathology, Fudan University Shanghai Cancer Center, 270 Dong An Road, Shanghai 200032, China. Phone & Fax +86 21 6417 5590. E-mail xyzhou100@163.com

No potential conflicts of interest were disclosed.

Running title: HDAC6 activates MET signaling in DLBCL.

Funding: This work was supported by the National Nature Science Funding of China (NSFC; Code Nos. 81272630 and 81470353) and the Shanghai Key Developing Disciplines (Code No. 2015ZB0201).

Word count for text: 4,020

Word count for abstract: 178

Abstract

Some histone deacetylases (HDACs) promote tumor cell growth and pan- or selective HDAC inhibitors are active in some cancers, however, the pivotal HDAC enzyme and its functions in human diffuse large B-cell lymphoma (DLBCL) remain largely unknown. Using NanoString nCounter assays, we profiled *HDAC* mRNA expression and identified *HDAC6* as an upregulated HDAC family member in DLBCL tissue samples. We then found that HDAC6 plays an oncogenic role in DLBCL, as evidenced by its promotion of cell proliferation *in vitro* and tumor xenograft growth *in vivo*. Mechanistically, the interaction between HDAC6 and HR23B downregulated HR23B expression, thereby reducing the levels of casitas B-lineage lymphoma (c-Cbl), an E3 ubiquitin ligase for hepatocyte growth factor receptor (MET), which resulted in the inhibition of MET ubiquitination-dependent degradation. In addition, enhanced HDAC6 expression and decreased HR23B expression were correlated with poor overall survival rates among patients with DLBCL. Taken together, these results establish an HDAC6-HR23B-MET axis and indicate that HDAC6 is a potent promoter of lymphomagenesis in DLBCL. Thus, a therapeutic strategy based on HDAC6 inhibitors in combination with MET inhibitors is promising.

Keywords DLBCL; HDAC6; HR23B; HGF/MET

Introduction

The pathogenesis of human diffuse large B-cell lymphoma (DLBCL) is complex and heterogeneous, and the potential pathogenic mechanisms have not been fully elucidated [1]. In addition to genetic and genomic alterations, histone deacetylation, CpG methylation and histone hypermethylation contribute to chromatin remodeling/condensation and transcriptional inhibition of target genomic regions [2, 3]. Notably, histone deacetylases (HDACs) affect the transcription of many suppressor genes and oncogenes involved in cell proliferation, apoptosis, survival, differentiation, and genetic stability [4]. Histone modification changes are common in human malignancies, including DLBCL [5-7]. Inhibition of HDAC activity exerts potent *in vitro* antitumor effects and slows tumor xenograft growth *in vivo* [8,9]. Therefore, HDAC family members have become promising therapeutic targets.

Histone deacetylase 6 (HDAC6) is involved in the aggresomal degradation of ubiquitinated proteins and contributes to the sensitivity of HDAC inhibitors (HDACi) [9]. Deletion of HDAC6 delayed disease progression in an $SOD1^{G93A}$ mouse model of amyotrophic lateral sclerosis [10]. Additionally, HDAC6 deficiency has been shown to significantly suppress cell proliferation and prolong tumor xenograft growth in ovarian and prostate cancers [8,9]. Some studies have described the expression of HDAC6 in B- and T-cell lymphomas [5-7], although its clinical significance and functional role in

lymphomagenesis and subsequent progression remain largely unknown. A recent study revealed that HDAC6 downregulates HR23B by interacting with it, thereby inducing the apoptosis of desensitizing cells by decreasing the levels of ubiquitinated substrates that are targeted to the proteasome [11]. HR23B (encoded by *RAD23B*), which has been previously identified as a biomarker in response to HDACi [12-14], can function as a tumor suppressor [15]. Furthermore, HR23B targets gene promoters, which implies that HR23B might be involved in transcriptional regulation [16]. Hence, the function of HR23B in mediating HDAC6 to regulate its downstream signaling should be further explored.

Hepatocyte growth factor receptor (MET) is involved in various biological processes, including cell proliferation, migration, invasion and dissemination, in many human cancers [17-20]. MET has been found to be overexpressed in patients with DLBCL and correlated with upregulation of phosphorylated Akt (p-Akt) and phosphorylated GSK3 (p-GSK3); *in vitro*, MET inhibition by either pharmacological or genetic means leads to caspase-dependent apoptosis [17]. Studies of MET signaling in hepatocellular carcinoma (HCC) have revealed that MET tyrosine kinase signaling is regulated and hyperactivated by HDACs through microRNA-449 inhibition [3]. However, the relationship between HDACs and MET signaling and alternative mechanisms have not been investigated in DLBCL.

Ricolinostat is the first oral selective HDAC6 inhibitor with reduced class I HDAC activity to be studied clinically, and it might partner well with other compounds to enhance

their efficacies in treating diverse cancers. Although the results from experimental or preclinical studies have shown that combinations of ricolinostat with lenalidomide, ibrutinib, carfilzomib or bortezomib can exerts synergistic effects in multiple myeloma, DLBCL and mantle cell lymphoma [21-26], the combination of ricolinostat with a MET inhibitor (METi) has not been investigated in DLBCL.

Based on the aforementioned observations, we aimed to determine whether HDAC6 plays a key role in lymphomagenesis and whether HR23B is essential for HDAC6-mediated regulation of MET signaling in DLBCL.

Materials and methods

Patient samples

After obtaining approval from the institutional review boards and the local ethical committees from the authors' institutions, 87 fresh-frozen and 151 paraffin-embedded tumor biopsy samples from patients with DLBCL, along with 12 fresh-frozen and 20 paraffin-embedded non-tumor lymphoid tissue samples from individuals who were diagnosed with reactive lymphoid hyperplasia (RLH), were collected from Fudan University Shanghai Cancer Center (Shanghai, China). Informed consent was obtained from the participants who provided specimens. DLBCL was identified as the germinal center B-cell (GCB) or the

activated B-cell (ABC) subtype based on the Hans immunohistochemistry (IHC) algorithm for fresh/frozen paraffin-embedded tumor biopsies [27,28]. The RLH samples, including tonsils and lymph nodes, were obtained from individuals who underwent tonsillectomies or lymph node biopsies. For *HDAC* expression profiling in DLBCL, total RNA was isolated from 24 enriched DLBCL frozen tumor tissues and 10 tonsil tissues and was subjected to NanoString nCounter assays. *HDAC6* mRNA expression was further detected in a larger validation cohort of 87 DLBCL and 12 RLH samples, including the discovery cohort, by using RT-qPCR. Representative histological FFPE blocks of 151 DLBCL tumor biopsies, including 58 DLBCL samples from the above validation cohort and 20 RLH samples, were subjected to IHC analysis.

NanoString nCounter assay

HDAC expression profiling was conducted for 24 enriched DLBCL tumor samples and 10 tonsil samples using NanoString nCounter assays (NanoString Technologies, Seattle, WA, USA) with a panel of custom-compiled gene probes, including total *HDAC*s (*HDAC1-11* and *SIRT1-7*). The custom array contained 18 gene probes with three "housekeeping" reference genes (*ALAS1, B2M* and *CLTC*), which were used as the internal controls (supplementary material, Table S1). A NanoString assay was performed as previously described [29]. For a detailed description, see supplementary material, Supplementary materials and methods.

A NanoString nCounter assay was also performed to investigate the potential signaling downstream of HDAC6, as described above. Based on a comprehensive review of the most recent and most significant references, we designed a library containing the 79 genes found in several pivotal pathways that might play key roles in the initiation, progression and therapeutic target development of DLBCL in addition to three reference genes by generating a probe array (supplementary material, Table S1).

Cell lines and lentiviral infection

NuDUL1, SuDHL-2 and SuDHL-4 cells were purchased from the American Type Culture Collection (ATCC, USA). OCI-LY1, OCI-LY8 and OCI-LY10 were kindly provided by Dr. B. Hilda Ye (Albert Einstein College of Medicine, NY, USA), and the DoHH2 cells were a gift from Prof. Mingzhi Zhang (the First Affiliated Hospital of Zhengzhou University, Zhengzhou, China). Toledo cells were provided as a gift from Dr. Thomas Wu (Sundia MediTech, Shanghai, China). All cell lines were authenticated through short tandem repeat profiling at SIBS (Shanghai, China) and tested for mycoplasma infection using the Universal Mycoplasma Detection Kit (ATCC). Generation of cells stably transfected with lentivirus was performed (supplementary material, Supplementary materials and methods).

RT-qPCR

Total RNA was isolated using a TRIzol kit (Invitrogen, Grand Island, NY, USA) and purified with an RNeasy Plus Kit (Qiagen, San Diego, CA, USA). cDNA was synthesized with the M-MLV Reverse Transcriptase Kit (Invitrogen). Then, qPCR was performed using SYBR GREEN according to a standard protocol (Takara, Shiga, Japan). For a detailed description, see supplementary material, Supplementary materials and methods.

Histological and cytological staining

Histological processing and staining and immunofluorescence (IF) staining were performed as described previously [18] and in supplementary material, Supplementary materials and methods.

Using a histological scoring system, the results of IHC for HDAC6 and HR23B were determined. Both staining intensity and the proportion of positive tumor cells were taken into account. Briefly, a proportional score of 0 to 4 was assigned for the proportion of positive cells (0, no positive cells; 1, ≤ 25% positive cells; 2, 26~50% positive cells; 3, 51~75% positive cells; 4, > 75% positive cells). An intensity score of 0 to 3 was assigned for the intensity of positive cells (0, none; 1, weak; 2, intermediate; 3, strong). The final score was clustered into four groups: "-" denotes ≤ 2 total points; "+" denotes 3-4 total points; "++" denotes 5-6 total points; "+++" denotes 7 total points. Additionally, "-" and "+" are defined as low expression, whereas "++" and "+++" are defined as high expression [14].

Western blot and immunoprecipitation (IP)

Frozen human DLBCL tissues or harvested cells were lysed with RIPA lysis buffer. Western blot and IP assays were performed as described previously [18]. Details of primary and secondary antibodies are shown in supplementary material, Table S2.

Cell proliferation and apoptosis

Cell number was monitored using a Cell Counting Kit-8 (CCK8; Dojindo, Kumamoto, Japan) according to the manufacturer's instructions. Apoptosis was detected using a dual staining Annexin V/PE-7AAD Apoptosis Detection kit (BD Biosciences, San Diego, CA, USA) and a Cytomics FC500 flow cytometer (Beckman Coulter, Brea, CA, USA). The percentage of apoptotic cells in each quadrant was analyzed using CXP Software (Beckman Coulter). Each experiment was performed in triplicate.

Tumor xenograft models

The animal studies were performed under the guidelines approved by the Animal Ethics Boards of Fudan University Shanghai Cancer Center. We established animal models based on previous studies [30-32]. In brief, female 6-week-old BALB/c nude mice were randomly assigned to four groups (n = 6 per group) and anesthetized through intraperitoneal (i.p.)

injection of ketamine (100 mg/kg). Subsequently, the mice were injected subcutaneously (s.c.) with 2×10^6 NuDUL-1 cells infected with either Lenti-shHDAC6 or negative control (NC) in 0.05 ml of PBS or injected with OCI-LY8 cells infected with either Lenti.HDAC6 or NC in 0.05 ml of PBS. The tumor volumes were estimated by measuring two dimensions (length [L] and width [W]), and the volume was calculated as $V = LW^2 / 2$. Finally, the tumors were excised and frozen in liquid nitrogen or fixed in 4% neutral paraformaldehyde solution for Western blot or IHC analyses, respectively.

Additionally, NuDUL-1 cells without any treatment were injected into 24 mice, and when the tumors reached 68–185 mm^3, the mice were randomly assigned to four groups (n = 6 per group). We intraperitoneally treated the mice every other day with the vehicle (DMSO), with crizotinib and ricolinostat (Selleck Chemicals; 50 mg per kg body weight) through daily oral gavage [22,33], or with the ricolinostat/crizotinib combination for 18 d. In addition to tumor volume estimation, the tumor doubling time (DT) and tripling time (TT) were calculated. For all procedures (implantation and chemotherapy), the mice were anesthetized with an i.p. injection of ketamine/xylazine (87/13 mg/ml) at 1 ml/kg. For implantation, the mice were anesthetized with an i.p. injection of ketamine/xylazine (87/13 mg/ml) at 1 ml/kg. Finally, all mice were euthanized by cervical dislocation under anesthesia.

Statistical analysis

The statistical analyses were performed using GraphPad Prism v 7.0 (GraphPad Software, La Jolla, CA, USA). The data, presented as the means ± SDs, were analyzed using unpaired two-tailed Student's t-tests or one-way analysis of variance (ANOVA). Kaplan-Meier survival curves were plotted, and a log-rank test was performed. For drug-synergy assessment, the combination index (CI) was calculated using CompuSyn v 1.0 (ComboSyn, Paramus, NJ, USA). Two-sided p values < 0.05 were considered significant, and CI < 1.0 was considered to indicate synergism.

Results

HDAC6 is differentially expressed in DLBCL tissues and associated with poor prognosis

Using NanoString nCounter assays, we identified *HDAC1* and *HDAC6* as the top two differentially expressed *HDAC* mRNAs in 24 DLBCL patient samples, while *HDAC6* expression was five-fold higher in the 24 DLBCL tissues than in the 10 tonsil tissues (Figure 1A). To validate this finding, RT-qPCR was performed using 87 DLBCL and 12 RLH samples, including the samples tested by NanoString nCounter assays. Consistently, *HDAC6* mRNA expression was significantly higher in the DLBCL tissues than in the RLH tissues ($p < 0.05$; Figure 1B). Western blot analysis established that HDAC6 protein expression was higher in DLBCL than in RLH (Figure 1C). IHC analysis of 151 DLBCL samples revealed that HDAC6 was localized in the perinuclear/cytoplasmic region and was differentially

expressed in DLBCL; however, HDAC6 expression was primarily limited to germinal centers (GCs) in RLH samples (Figure 1D). The IHC revealed that high HDAC6 expression was found in 32% (48/151) of the DLBCL samples, which was significantly more frequently than in the RLH samples (10%, 2/20) ($p < 0.05$, Figure 1E). Meanwhile, the expression levels of HDAC6 were comparable between NanoString and RT-qPCR ($p < 0.05$, supplementary material, Figure S1A) and between RT-qPCR and IHC ($p < 0.05$). However, no significant correlation between the results from NanoString and IHC was observed ($p > 0.05$), which could be due to the limited overlapping samples.

The clinicopathological features of 151 DLBCL samples grouped by HDAC6 protein expression levels as determined by IHC are summarized in supplementary material, Table S3. High HDAC6 protein expression ($HDAC6^{high}$) was associated with tumor stage progression ($p < 0.05$). Kaplan-Meier survival curves, with a median follow-up of 30 months, demonstrated that the overall survival (OS) of DLBCL patients bearing tumors with $HDAC6^{high}$ was substantially lower than that of DLBCL patients bearing tumors with low HDAC6 protein expression ($HDAC6^{low}$) ($p < 0.001$, Figure 1F). Multivariate Cox regression analysis revealed that high HDAC6 expression was associated with poor prognosis in DLBCL (hazard ratio, 3.48; $p < 0.001$), and HDAC6 is an independent prognostic factor in DLBCL (supplementary material, Table S4).

HDAC6 knockdown arrests cell proliferation and triggers cell cycle arrest and apoptosis in DLBCL cells

Given the correlation of high HDAC6 expression with poor prognosis in DLBCL, we sought to explore the functional impact of HDAC6 in DLBCL cells. Western blot analysis showed that HDAC6 was highly expressed in all non-GCB/ABC-subtype cell lines (NuDUL-1, OCI-LY10 and SuDHL-2 cells) and in one GCB-subtype cell line, Toledo cells (Figure 2A). NuDUL-1 and Toledo cells were infected with Lenti-shHDAC6, while Lenti-HDAC6 infection was performed in OCI-LY1 and OCI-LY8 cells with lower basal HDAC6 expression. Knockdown of HDAC6 in NuDUL-1 and Toledo cells significantly abrogated cell proliferation, whereas overexpression of HDAC6 in OCI-LY1 and OCI-LY8 cells revealed opposite effects (Figure 2B). A fluorescence-activated cell sorting (FACS) analysis revealed that knockdown of HDAC6 induced a significant increase in early apoptosis in NuDUL-1 and Toledo cells, whereas HDAC6 overexpression did not induce significant opposite effects (Figure 2C). Consistently, knockdown of HDAC6 in NuDUL-1 and Toledo cells resulted in increased cleaved PARP and cleaved caspase-9, -8, and -3 expression (Figure 2D), whereas except for a reduction in cleaved PARP expression observed in OCI-LY8 cells with HDAC6 overexpression, no obvious changes in the protein levels were found in OCI-LY1 or OCI-LY8 cells with HDAC6 overexpression (supplementary material, Figure S1B). Similarly, knockdown HDAC6 in NuDUL-1 and Toledo cells led to significant cell

arrest in the G2/M phase (Figure 2E), whereas HDAC6 overexpression did not induce opposite effects in OCI-LY1 or OCI-LY8 cells (supplementary material, Figure S1C). Changes in the representative regulatory proteins involved in cell cycle progression, including cyclin E1, CDK6, cyclin B1, p27 and p21, supported our findings by FACS analysis (Figure 2F; supplementary material, Figure S1D).

HDAC6 activates MET signaling in DLBCL

We sought to investigate the potential signaling pathways regulated by HDAC6. Using NanoString nCounter assays, we evaluated mRNA changes in selected genes associated with several pivotal signaling pathways (in terms of the initiation, progression and therapeutic target development of DLBCL) in stable HDAC6-downregulated NuDUL-1 cells. Genes associated with the HGF/MET pathway were significantly regulated in the HDAC6-knockdown groups compared to control groups (Figure 3A). We therefore evaluated MET protein expression in 151 DLBCL samples by IHC; MET was primarily localized on the cell membrane (Figure 3B) and was significantly increased in DLBCL tissues (28%, 42/151) compared to RLH tissues (10%, 2/20, Figure 3C). Increased HDAC6 and MET expression levels were found in some DLBCL samples by IHC, although no significant correlation was observed in the 151 DLBCL samples ($p > 0.05$). Western blot (Figure 3D) and IF (Figure 3E) analyses revealed that MET expression was decreased in the

HDAC6-downregulated NuDUL-1 and Toledo cells, whereas upregulation of HDAC6 in OCI-LY8 and OCI-LY1 cell lines produced opposite effects. Moreover, MET protein expression was significantly reduced in NuDUL-1 and Toledo cells treated with ricolinostat as determined by FACS analysis ($p < 0.001$, supplementary material, Figures S2A, B). MET is known as a potent activator of the PI3K/Akt and Ras/MAPK pathways and the NF-º B cascades [18]; therefore we measured total and phosphorylated protein expression levels of several members of these pathways. Knockdown of HDAC6 in NuDUL-1 and Toledo cells resulted in downregulation of phosphorylated Akt, NF-º B and Erk1/2, whereas phosphorylated NF-º B1 and NF-º B2 levels remained unaffected (Figure 3F).

HR23B deficiency mediates MET activation by HDAC6

In addition to serving as a response biomarker to HDACi, HR23B is a downstream regulator of HDAC6 [11]. Western blots and IF confirmed the correlation between HDAC6 and HR23B, and IP revealed that HR23B directly interacts with HDAC6 (supplementary material, Figures S3A-C). We therefore hypothesized that HR23B might mediate the activation of MET by HDAC6. By infecting NuDUL-1 and OCI-LY8 cells with Lenti-shHR23B and Lenti-HR23B, respectively, we accordingly observed upregulation and downregulation of MET protein by Western blot and IF (Figures 4A, B). Furthermore, HDAC6 knockdown increased HR23B and reduced MET expression in the DLBCL cells, whereas overexpression

of HDAC6 produced the opposite effect, as shown by the Western blot (Figure 4C). Previous studies have shown that casitas B-lineage lymphoma (c-Cbl), an E3-ubiquitin ligase for MET, plays a key role in regulating MET ubiquitination-dependent degradation [33,34]. Thus, we investigated whether HR23B deficiency caused c-Cbl downregulation by assessing the levels of c-Cbl and global ubiquitination in HR23B-knockdown cells and in cells overexpressing HR23B. The knockdown of HR23B in NuDUL-1 cells resulted in lower levels of c-Cbl and global ubiquitination expression than those in the control cells, and the opposite effects were observed in HR23B-overexpressing OCI-LY8 cells (Figure 4D).

In addition, we assessed HR23B expression in 151 DLBCL clinical tissue samples using IHC. HR23B was differentially expressed in DLBCL and was scored as “low” or “high” (Figure 4E). The frequency of high HR23B expression (68%, 103/151) in DLBCL tissues was significantly lower than that in RLH tissues (95%, 19/20) ($p < 0.05$, Figure 4F). Significant associations were found between low HR23B expression and more aggressive phenotypes (high International Prognostic Index [IPI] scores and ABC type; supplementary material, Table S3). Kaplan-Meier survival curves revealed a lower OS rate for DLBCL patients with HR23B deficiency ($p < 0.05$, Figure 4G), although multivariate Cox regression analysis showed that HR23B expression was not an independent prognostic factor for DLBCL (data not shown). As indicated by IHC and Western blot analyses, HDAC6 expression was negatively correlated with HR23B expression in the 151 DLBCL samples

(supplementary material, Figures S4A-C, $r = -0.375$, $p < 0.001$). Furthermore, HR23B expression was significantly positively correlated with MET expression in the 151 DLBCL samples ($p < 0.05$).

MET inhibition increased the inhibitory effect induced by HDAC6i in DLBCL cells

The aforementioned findings established an HDAC6-HR23B-MET axis, which led us to evaluate the combinatorial effect of inhibitors targeting HDAC6 and MET in DLBCL. Through Lenti-shHDAC6 and Lenti-shMET transfection, we first determined that the knockdown of MET increased the inhibitory effects of the HDAC6 knockdown in NuDUL-1 and Toledo cells (Figure 5A). We then selected ricolinostat and crizotinib, a potent inhibitor of MET, for treating $HDAC6^{high}$ NuDUL-1 and Toledo cells. The IC_{50} values of ricolinostat and crizotinib were determined from dose-response studies using CCK8 assays. The single treatment with ricolinostat or crizotinib showed moderate efficacy in both NuDUL-1 and Toledo cells (Figure 5B), whereas another METi, PF-04217903, was not active in either DLBCL cell line (supplementary material, Figure S5). FACS analysis showed that ricolinostat induced apoptosis in DLBCL cells, which was also supported by Western blot analysis (Figures 5C and 5D). Importantly, compared with the effects of either inhibitor alone, the combination of ricolinostat and crizotinib exerted potent inhibition on DLBCL cell growth and generated strong synergistic effects (CI values < 1.0, Figures 5E and 5F). The

combination treatment induced apoptosis of NuDUL-1 and Toledo cells, as was also demonstrated by increased PARP cleavage and caspase-3 cleavage (Figures 5G and 5H). Moreover, the combination reduced the level of phosphorylated MET (Figure 5H).

***HDAC6 facilitated lymphomagenesis, and ricolinostat in combination with crizotinib generated a synergistic effect on DLBCL* in vivo**

Consistent with the *in vitro* findings, the knockdown of HDAC6 significantly arrested NuDUL-1 DLBCL xenograft growth by reducing the tumor size up to 85.5% compared with the NC ($p < 0.001$; Figure 6A). Staining for the proliferation marker Ki-67 also revealed significantly decreased expression in tumor cells (Figure 6B), whereas compared with the NC condition, HDAC6 overexpression increased OCI-LY8 xenograft growth by ~4.15-fold and increased Ki-67 expression (Figures 6C and 6D).

Subsequently we examined the *in vivo* efficacy of ricolinostat combined with crizotinib using a human DLBCL xenograft mouse model. The growth delay (GD) obtained with the combination of inhibitors was significantly longer than that observed in the groups treated with each inhibitor alone (DT, $p < 0.01$; TT, $p < 0.01$, Figure 6E). Crizotinib (50 mg/kg) and ricolinostat (50 mg/kg) modestly suppressed tumor growth by ~47% and ~62%, respectively, compared with DMSO treatment. Moreover, the combination treatment significantly inhibited tumor growth by ~87% (crizotinib/ricolinostat; Day 28, $p < 0.001$; Figure 6F). In

addition to GD and tumor size, we also assessed the effects of the treatments on total and phosphorylated MET protein expression and the expression of the proliferation marker Ki-67 (Figure 6G, supplementary material, Figure S6), which confirmed our *in vitro* findings. Taken together, the findings suggest that the combination of crizotinib and ricolinostat is a promising therapeutic strategy for DLBCL.

Discussion

HDAC6, a class IIb HDAC, acts as a deacetylase of ±-tubulin and other cytoplasmic proteins (*e.g.*, HSP90 and cortactin) [35,36]. HDAC6 plays critical roles in transcription regulation, cell cycle progression and tumor cell survival. Its selective inhibitors have been enrolled into clinical trials; however, the functions of HDAC6 in tumors remain controversial. Through activation of the JNK/c-Jun pathway, leading to autophagic cell death, or via suppression of NF-º B p65 nuclear translocation, causing inactivation of NF-º B signaling, HDAC6 has been characterized as a tumor suppressor in HCC [37]. Interestingly, high levels of HDAC6 mRNA and protein predict a better prognosis in patients with breast cancer, but forced expression of HDAC6 significantly increased cell motility and cell migration in breast cancer cells (MCF-7) [38, 39]. In a recent study, HDAC6 decreased cell migration and invasion abilities via deacetylation of heat-shock protein 5 (HSPA5), a marker of poor prognosis that promotes drug resistance and metastasis, at lysine residue 353 (K353) in breast cancer cells

[40]. Our findings demonstrate that HDAC6 plays an oncogenic role in DLBCL via indirect activation of MET signaling. Several reports have shown that HR23B can be used as a biomarker in response to HDACi; however, some studies have suggested a potential role for HR23B as a tumor suppressor in cancer progression. To date, little is known about the functions and mechanisms of HR23B in the initiation and subsequent progression of human malignancies. Recently, a novel function of HR23B was revealed: targeting gene promoters and performing transcriptional regulation [16]. The data presented here validate HR23B as a tumor suppressor-like factor that is inactivated by HDAC6 in DLBCL. Moreover, we found that decreased HR23B expression could serve as a prognostic factor in DLBCL, which is consistent with a previous study of breast cancer [15]. The results also confirmed that forced expression of HR23B inhibits cell proliferation and triggers apoptosis *in vitro*, suggesting that HR23B supports the tumor-suppressing role of HR23B in DLBCL. In this study, we first identified HR23B as a modulator of MET signaling. HR23B knockdown substantially upregulated MET expression, which is consistent with the effect induced by HDAC6 overexpression. HR23B is involved in ubiquitination-dependent degradation, and several previous reports have suggested that MET ubiquitination can be mediated by c-Cbl [33,34,41]. Therefore, we hypothesized that HR23B regulates c-Cbl and influences MET ubiquitination. We confirmed that HR23B upregulates c-Cbl, resulting in increased ubiquitination levels and reduced MET levels.

Despite the increasing knowledge base of genomic and transcriptomic abnormalities, a major clinical challenge persists: approximately 40% of patients with DLBCL receiving standard therapy of rituximab plus cyclophosphamide, doxorubicin, vincristine, and prednisolone (R-CHOP) are not cured [42]. To conquer this challenge, multiple targeted drugs have been developed and tested with one agent alone or in combination with other agents in clinical trials. Notably, the HDAC family, as the most important epigenetic modifier family, is responsible for chromatin remodeling, and has attracted considerable attention as a therapeutic target [3]. Similarly, most inhibitors or reagents, including those that inhibit HDAC or MET, those that are used for DLBCL treatment have shown limited efficacy when used alone, whereas their combination with other drugs might exert a synergistic antitumor effect [43-45]. After validating the efficacy of the combined ricolinostat and crizotinib treatment *in vitro*, we confirmed that the combination inhibits DLBCL xenograft growth *in vivo*.

Taken together, our findings demonstrate that HDAC6 plays an oncogenic role in DLBCL pathogenesis and could serve as a prognostic marker for DLBCL. The established HDAC6-HR23B-MET axis is associated with the oncogenic function of HDAC6 and provides a rationale for the use of ricolinostat and crizotinib combination treatment for patients with DLBCL.

Acknowledgments

We acknowledge Prof. W. Yang (Vice Chief of the Department of Pathology, Fudan University Shanghai Cancer Center) for critical discussions and helpful editorial advice. We thank Prof. Q. Liu (Chief of the Department of Pathology, Renji Hospital, School of Medicine, Shanghai Jiao Tong University) for constant support of this project. This work was supported by grants from the National Natural Science Foundation of China (NSFC; Code Nos. 81272630 and 81470353) and the Shanghai Key Developing Disciplines Program (Code No. 2015ZB0201). We thank American Journal Experts for their assistance with language revision.

Author contributions statement

Z.L., Y.C. and Y.Y. performed the animal and *in vitro* studies and drafted the manuscript. A.L. and R.B. performed the IHC staining. L.W. and X.S. performed animal assay and analyzed the IHC data. W.W. and B.Y. performed the Western blot analysis and IP assays. B.C., W.C., Y.J. and P.W. participated in different parts of the animal and *in vitro* studies. X.Z. performed the statistical analyses and revised the manuscript. All authors read and approved the final manuscript.

References

1. Shipp MA, Ross KN, Tamayo P, *et al*. Diffuse large B-cell lymphoma outcome prediction by gene-expression profiling and supervised machine learning. *Nat Med* 2002; **8:** 68–74.

2. Bhalla KN. Epigenetic and chromatin modifiers as targeted therapy of hematologic malignancies. *J Clin Oncol* 2005; **23:** 3971–3993.

3. Buurman R, Gürlevik E, Schäffer V, *et al.* Histone deacetylases activate hepatocyte growth factor signaling by repressing microRNA-449 in hepatocellular carcinoma cells. *Gastroenterology* 2012; **143:** 811–820.e15.

4. Minucci S, Pelicci PG. Histone deacetylase inhibitors and the promise of epigenetic (and more) treatments for cancer. *Nat Rev Cancer* 2006; **6:** 38–51.

5. Gloghini A, Buglio D, Khaskhely NM, *et al.* Expression of histone deacetylases in lymphoma: implication for the development of selective inhibitors. *Br J Haematol* 2009; **147:** 515–525.

6. Marquard L, Poulsen CB, Gjerdrum LM, *et al.* Histone deacetylase 1, 2, 6 and acetylated histone H4 in B- and T-cell lymphomas. *Histopathology* 2009; **54:** 688–698.

7. Lee SH, Yoo C, Im S, *et al.* Expression of histone deacetylases in diffuse large B-cell lymphoma and its clinical significance. *Int J Med Sci* 2014; **11:** 994–1000.

8. Mak AB, Nixon AM, Kittanakom S, *et al.* Regulation of CD133 by HDAC6 promotes beta-catenin signaling to suppress cancer cell differentiation. *Cell Rep* 2012; **2:** 951–963.

9. Ai J, Wang Y, Dar JA, *et al.* HDAC6 regulates androgen receptor hypersensitivity and nuclear localization via modulating Hsp90 acetylation in castration-resistant prostate cancer. *Mol Endocrinol* 2009; **23:** 1963–1972.

10. Taes I, Timmers M, Hersmus N, *et al.* Hdac6 deletion delays disease progression in the SOD1G93A mouse model of ALS. *Hum Mol Genet* 2013; **22:** 1783–1790.

11. New M, Olzscha H, Liu G, *et al.* A regulatory circuit that involves HR23B and HDAC6 governs the biological response to HDAC inhibitors. *Cell Death Differ* 2013; **20:** 1306–1316.

12. Fotheringham S, Epping MT, Stimson L, *et al.* Genome-wide loss-of-function screen reveals an important role for the proteasome in HDAC inhibitor-induced apoptosis. *Cancer Cell* 2009; **15:** 57–66.

13. Khan O, Fotheringham S, Wood V, *et al.* HR23B is a biomarker for tumor sensitivity to HDAC inhibitor-based therapy. *Proc Natl Acad Sci USA* 2010; **107:** 6532–6537.

14. Yeo W, Chung HC, Chan SL, *et al.* Epigenetic therapy using belinostat for patients with unresectable hepatocellular carcinoma: a multicenter phase I/II study with biomarker and pharmacokinetic analysis of tumors from patients in the Mayo Phase II Consortium and the Cancer Therapeutics Research Group. *J Clin Oncol* 2012; **30:** 3361–3367.

15. Linge A, Maurya P, Friedrich K, *et al.* Identification and functional validation of RAD23B as a potential protein in human breast cancer progression. *J Proteome Res* 2014; **13:** 3212–3222.

16. Cattoglio C, Zhang ET, Grubisic I, *et al.* Functional and mechanistic studies of XPC DNA-repair complex as transcriptional coactivator in embryonic stem cells. *Proc Natl Acad Sci U S A* 2015; **112:** E2317–E2326.

17. Uddin S, Hussain AR, Ahmed M, *et al.* Inhibition of c-MET is a potential therapeutic strategy for treatment of diffuse large B-cell lymphoma. *Lab Invest* 2010; **90:** 1346–1356.

18. Liu Z, Wei P, Yang Y, *et al.* BATF2 deficiency promotes progression in human colorectal cancer via activation of HGF/MET signaling: A potential rationale for combining MET inhibitors with IFNs. *Clin Cancer Res* 2015; **21:** 1752–1763.

19. Ha SY, Lee J, Kang SY, *et al*. MET overexpression assessed by new interpretation method predicts gene amplification and poor survival in advanced gastric carcinomas. *Mod Pathol* 2013; **26:** 1632–1641.

20. Zagouri F, Bago-Horvath Z, Rössler F, *et al.* High MET expression is an adverse prognostic factor in patients with triple-negative breast cancer. *Br J Cancer* 2013; **108:** 1100–1105.

21. Amengual JE, Johannet P, Lombardo M, *et al.* Dual targeting of protein degradation pathways with the selective HDAC6 inhibitor ACY-1215 and Bortezomib is synergistic in lymphoma. *Clin Cancer Res* 2015; **21:** 4663–4675.

22. Dasmahapatra G, Patel H, Friedberg J, *et al.* In vitro and in vivo interactions between the HDAC6 inhibitor ricolinostat (ACY1215) and the irreversible proteasome

inhibitor carfilzomib in non-Hodgkin lymphoma cells. *Mol Cancer Ther* 2014; **13:** 2886–2897.

23. Mishima Y, Santo L, Eda H, *et al.* Ricolinostat (ACY-1215) induced inhibition of aggresome formation accelerates carfilzomib-induced multiple myeloma cell death. *Br J Haematol* 2015; **169:** 423–434.

24. Yee AJ, Bensinger WI, Supko JG, *et al.* Ricolinostat plus lenalidomide, and dexamethasone in relapsed or refractory multiple myeloma: a multicentre phase 1b trial. *Lancet Oncol* 2016; **17:** 1569–1578.

25. Amengual JE, Prabhu SA, Lombardo M, *et al.* Mechanisms of acquired drug resistance to the HDAC6 selective inhibitor Ricolinostat reveals rational drug-drug combination with Ibrutinib. *Clin Cancer Res* 2017; **23:** 3084–3096.

26. Santo L, Hideshima T, Kung AL, *et al.* Preclinical activity, pharmacodynamic, and pharmacokinetic properties of a selective HDAC6 inhibitor, ACY-1215, in combination with bortezomib in multiple myeloma. *Blood* 2012; **119:** 2579–2589.

27. Hans CP, Weisenburger DD, Greiner TC, *et al.* Confirmation of the molecular classification of diffuse large B-cell lymphoma by immunohistochemistry using a tissue microarray. *Blood* 2004; **103:** 275–282.

28. Pore D, Bodo J, Danda A, *et al.* Identification of Ezrin-Radixin-Moesin proteins as novel regulators of pathogenic B-cell receptor signaling and tumor growth in diffuse large B-cell lymphoma. *Leukemia* 2015; **29:** 1857–1867.

29. Geiss GK, Bumgarner RE, Birditt B, *et al.* Direct multiplexed measurement of gene expression with color-coded probe pairs. *Nat Biotechnol* 2008; **26:** 317–325.

30. Dai B, Zhao XF, Mazan-Mamczarz K, *et al.* Functional and molecular interactions between ERK and CHK2 in diffuse large B-cell lymphoma. *Nat Commun* 2011; **2:** 402.

31. Souers AJ, Leverson JD, Boghaert ER, *et al.* ABT-199, a potent and selective BCL-2 inhibitor, achieves antitumor activity while sparing platelets. *Nat Med* 2013; **19:** 202–208.

32. Kentsis A, Reed C, Rice KL, *et al.* Autocrine activation of the MET receptor tyrosine kinase in acute myeloid leukemia. *Nat Med* 2012; **18:** 1118–1122.

33. Qin S, Taglienti M, Nauli SM, *et al.* Failure to ubiquitinate c-Met leads to hyperactivation of mTOR signaling in a mouse model of autosomal dominant polycystic kidney disease. *J Clin Invest* 2010; **120:** 3617–3628.

34. Wei TT, Lin YC, Lin PH, *et al.* Induction of c-Cbl contributes to anti-cancer effects of HDAC inhibitor in lung cancer. *Oncotarget* 2015; **6:** 12481–12492.

35. Kovacs JJ, Murphy PJ, Gaillard S, *et al.* HDAC6 regulates Hsp90 acetylation and chaperone-dependent activation of glucocorticoid receptor. *Mol Cell* 2005; **18:** 601–607.

36. Nakashima H, Kaufmann JK, Wang PY, *et al.* Histone deacetylase 6 inhibition enhances oncolytic viral replication in glioma. *J Clin Invest* 2015; **125:** 4269–4280.

37. Bae HJ, Jung KH, Eun JW, *et al.* MicroRNA-221 governs tumor suppressor HDAC6 to potentiate malignant progression of liver cancer. *J Hepatol* 2015; **63:** 408–419.

38. Saji S, Kawakami M, Hayashi S, *et al.* Significance of HDAC6 regulation via estrogen signaling for cell motility and prognosis in estrogen receptor-positive breast cancer. *Oncogene* 2005; **24:** 4531–4539.

39. Zhang Z, Yamashita H, Toyama T, *et al.* HDAC6 Expression is correlated with better survival in breast cancer. *Clin Cancer Res* 2004; **10:** 6962–6968.

40. Chang YW, Tseng CF, Wang MY, *et al.* Deacetylation of HSPA5 by HDAC6 leads to GP78-mediated HSPA5 ubiquitination at K447 and suppresses metastasis of breast cancer. *Oncogene* 2016; **35:** 1517–1728.

41. Taher TE, Tjin EP, Beuling EA, *et al.* c-Cbl is involved in Met signaling in B cells and mediates hepatocyte growth factor-induced receptor ubiquitination. *J Immunol* 2002; **169:** 3793–3800.

42. Chan FC, Telenius A, Healy S, *et al.* An RCOR1 loss–associated gene expression signature identifies a prognostically significant DLBCL subgroup. *Blood* 2015; **125:** 959‑966.

43. Kalac M, Scotto L, Marchi E, *et al.* HDAC inhibitors and decitabine are highly synergistic and associated with unique gene-expression and epigenetic profiles in models of DLBCL. *Blood* 2011; **118:** 5506–5516.

44. Ciamporcero E, Miles KM, Adelaiye R, et al. Combination strategy targeting VEGF and HGF/c-met in human renal cell carcinoma models. *Mol Cancer Ther* 2015; **14:** 101–110.

45. Chakraborty AR, Robey RW, Luchenko VL, *et al.* MAPK pathway activation leads to Bim loss and histone deacetylase inhibitor resistance: rationale to combine romidepsin with an MEK inhibitor. *Blood* 2013; **121:** 4115–4125.

Figure legends

Figure 1. HDAC profiling identified HDAC6, a predictor of poor prognosis in DLBCL. (A) Heat map of the expression patterns of *HDAC* mRNAs (*HDAC1-11* and *Sirt1-7*) in 24 DLBCL and 10 RLH (tonsil) tissues, as detected through a NanoString nCounter assay. The relative enhancement of *HDAC* mRNA expression is indicated through a red-to-blue color gradient. (B) Further validation of *HDAC6* mRNA expression in 87 DLBCL and 12 RLH samples by RT-qPCR. Two-tailed Student's t test: * $p < 0.05$. (C) Representative Western blots showing HDAC6 expression in lysates from freshly collected DLBCL and RLH tissues. Glyceraldehyde 3-phosphate dehydrogenase (GAPDH) was used as a loading control. (D) Representative HDAC6 immunostaining in paraffin-embedded DLBCL tumor samples (scale bar = 20 μm) and RLH samples (scale bar = 20 μm). "GC" refers to germinal center. (E) Frequency of HDAC6 protein expression in 20 RLH tissues and 151 DLBCL tissue samples. Two-sided Chi-squared test: * $p < 0.05$. (F) Kaplan-Meier survival curves for patients with DLBCL and low expression (n = 103) and high expression (n = 48) of HDAC6 protein. RLH, reactive lymphoid hyperplasia. Two-sided log-rank test: $p < 0.001$. Error bars show SD.

Figure 2. Potential oncogenic role of HDAC6 in DLBCL. (A) The baseline of HDAC6 protein expression in eight DLBCL cell lines was determined through Western blot analysis. GAPDH was used as a loading control. (B) The proliferation of NuDUL-1 and Toledo cells

after infection with Lenti-shHDAC6 and OCI-LY1 and OCI-LY8 cells after infection with Lenti.HDAC6 was determined by CCK8 assays. The *p* value for each time point was calculated using a two-tailed Student's t test. * $p < 0.05$, ** $p < 0.01$, *** $p < 0.001$. (C) Assessment of apoptosis by Annexin V/PE-7AAD dual staining in NuDUL-1 and Toledo cells subjected to Lenti-shHDAC6 infection or OCI-LY1 and OCI-LY8 infected with Lenti.HDAC6 for 48 h. Each experiment was repeated three times. The *p* values were calculated using a two-tailed Student's t test. ** $p < 0.01$, *** $p < 0.001$. (D) The cleavage of PARP, caspase-3, caspase-8 and caspase-9 were detected in cells transduced with Lenti-shHDAC6 by Western blot analysis. GAPDH served as loading control. (E) Analysis of cell cycle progression by propidium iodide (PI) staining in indicated cells infected with Lenti-shHDAC6 and Lenti.HDAC6. Each experiment was repeated three times. (F) Western blot analyses of the levels of cyclin E1, CDK6, cyclin B1, P27 and P21 in NuDUL-1 and Toledo cells subjected HDAC6 knockdown or NC. GAPDH served as loading control. NC = negative control. CCK8 = Cell Counting Kit-8.

Figure 3. HDAC6 activates MET signaling in DLBCL. (A) A NanoString nCounter assay was used for pathway analysis between NuDUL-1 cells infected with Lenti-shHDAC6 and the NC. (B) Representative MET immunostaining in paraffin-embedded DLBCL tumor samples (scale bar = 20 μm) and RLH tissues (scale bar = 20 μm). The results were

determined by two pathologists who were both blinded to identifying information. The definition of "Low" or "High" expression was based on Uddin's work [17]. (C) Proportions of MET protein expression in RLH and DLBCL tissues. Two-sided chi-squared test: * $p <$ 0.05. (D) Extracts prepared from indicated cells infected with Lenti-shHDAC6 or Lenti.HDAC6 were assessed by Western blot analysis for MET protein. GAPDH served as a loading control. (E) Immunofluorescence of MET in stable HDAC6 shRNA-expressing or HDAC6-overexpressing cells. The localization and levels of MET expression were detected using a Leica TCS SP5 laser-scanning confocal microscope (scale bar = 25 μm). Cells were counterstained with DAPI (blue) for nuclear staining. (F) Western blot analysis for total and phosphorylated Akt, Erk1/2, NF-º B2, and NF-º B1 in lysates from NuDUL-1 and Toledo cells infected with Lenti-shHDAC6 and NC. GAPDH served as a loading control.

Figure 4. HR23B deficiency mediates MET activation by HDAC6. (A) Representative Western blots for HR23B and MET in NuDUL-1 and OCI-LY8 cells infected with Lenti-shHR23B and Lenti.HR23B, respectively. (B) Immunofluorescence staining for MET in stable HR23B shRNA-expressing NuDUL-1 cells and HR23B-overexpressing OCI-LY8 cells was analyzed using a Leica TCS SP5 laser-scanning confocal microscope (scale bar = 25 μm). The cells were counterstained with DAPI (blue) for nuclear staining. (C) Representative Western blots for HDAC6, HR23B and MET in NuDUL-1, and OCI-LY8

cells infected with Lenti-shHDAC6 and Lenti.HDAC6, respectively. (D) Lysates from cells treated with Lenti-shHDAC6 or Lenti.HR23B and NC were analyzed by Western blot with anti-c-Cbl, anti-Ub, and anti-MET antibodies for the detection of c-Cbl, ubiquitination and MET, respectively. NC = negative control. Ub = ubiquitin. (E) Immunostaining for HR23B in 20 RLH tissues and 151 DLBCL tissue samples. Two-sided Chi-squared test: * $p < 0.05$. (F) Proportions of HR23B protein expression in RLH and DLBCL tissues. Two-sided Chi-squared test: * $p < 0.05$. (G) Kaplan-Meier survival curves for patients with DLBCL and low and high expression of HR23B protein. Two-sided log-rank test: $p < 0.05$.

Figure 5. MET inhibition increases the inhibitory effects triggered by HDAC6 suppression *in vitro*. (A) Cell proliferation in NuDUL-1 and Toledo cells infected with Lenti-shHDAC6, Lenti-shMET or both was monitored by CCK8 assays. ** $p < 0.01$, *** $p < 0.001$. (B) Calculation of IC_{50} values for ricolinostat and crizotinib in NuDUL-1 and Toledo cells based on CCK8 assays. (C) Assessment of apoptosis by Annexin V/PE-7AAD dual staining of cells treated with ricolinostat. Vehicle was compared with ricolinostat using two-tailed Student's t test: * $p < 0.05$. Each experiment was repeated three times. (D) Extracts prepared from NuDUL-1 and Toledo cells treated with ricolinostat were analyzed by Western blotting with anti-PARP or anti-cleaved caspase-3 (C-caspase-3) antibodies. GAPDH served as a loading control. (E) Cell proliferation of NuDUL-1 cells treated with ricolinostat (1 μM), crizotinib

(13 μM), or both, and of Toledo cells treated with ricolinostat (2.5 μM), crizotinib (75 μM), or both was monitored through CCK8 assays. One-way ANOVA: * $p < 0.05$. (F) Calculation of the combination index (CI) values for each pair of concentrations with fixed molar-ratio combinations of ricolinostat and crizotinib in NuDUL-1 cells and Toledo cells. (G) Using the identical drug concentrations described above, the assessment of apoptosis was performed through Annexin V/PE-7AAD dual staining of cells treated with ricolinostat, crizotinib or both. One-way ANOVA: * $p < 0.05$. Each experiment was repeated three times. (H) Western blot analysis of PARP, C-caspase-3, total MET and phosphorylated MET (p-MET) in NuDUL-1 and Toledo cells treated as previously described. GAPDH served as a loading control. NC = negative control.

Figure 6. HDAC6 promotes tumor growth, and combined crizotinib and ricolinostat treatment produces synergistic effects *in vivo*. (A) Twelve BALB/c nude mice were randomly assigned into two groups of 6 and injected with NuDUL-1 cells infected with Lenti-shHDAC6 or NC. Representative tumors were imaged to visually assess tumor growth (*left*). The average tumor volume in each group (n = 6 per group) is shown as a function of time (*right*). The *p* value was calculated using a two-tailed Student's t test. ** $p < 0.01$. (B) Immunostaining for the proliferation marker Ki-67 and conventional H&E staining (*left*) in tissues from DLBCL xenograft mice treated as described in (A) (scale bar = 20 μm).

Quantification of Ki-67-positive lesions in tissues from the NC group and the shHDAC6 group (*right*). ** $p < 0.01$. (C) Lenti.HDAC6- or NC-infected OCI-LY8 cells were subcutaneously implanted into BALB/c nude mice (n = 6 per group), and the tumor growth was assessed as described in (A). ** $p < 0.01$. (D) Immunostaining for the proliferation marker Ki-67 and conventional H&E staining in tissues from DLBCL xenograft mice implanted with OCI-LY8 cells infected with Lenti.HDAC6 or NC (scale bar = 20 μm). Quantification of Ki-67-positive lesions in tissues from the NC group and the HDAC6 group. ** $p < 0.01$. NuDUL-1 cells not subjected to treatment were used to produce xenografts, and when tumors reached 68–185 mm^2 in size, the mice were grouped (n = 6 per group) and treated for 18 days as follows: crizotinib and ricolinostat (50 mg per kg body weight) were provided through daily oral gavage, and crizotinib combined with ricolinostat was administered. (E) The effects of treatment with vehicle, crizotinib, ricolinostat or combination on tumor growth in NuDUL-1 xenografts were monitored according to the tumor DT and tripling time (TT). One-way ANOVA: ** $p < 0.01$. (F) Representative tumors were imaged after sacrifice to visually assess the efficacy of crizotinib, ricolinostat or the combination treatment on the tumor growth of NuDUL-1 xenografts in mice. At the final time point, the *p* value was calculated through one-way ANOVA: *** $p < 0.001$. (G) Western blot analyses confirmed a reduction of MET phosphorylation after the combination treatment with crizotinib and ricolinostat. GAPDH served as a loading control. Error bars show SD. NC =

negative control.

SUPPLEMENTARY MATERIAL ONLINE

Supplementary materials and methods YES

Supplementary figure legends YES

Figure S1. The detection of HDAC6 expression in DLBCL tissues and the effect of HDAC6 on apoptosis and cell cycle regulation in DLBCL cells

Figure S2. The selective HDAC6 inhibitor ricolinostat reduces the ratio of MET-expressing cells

Figure S3. Interaction of HDAC6 and HR23B down-regulates HR23B in DLBCL

Figure S4. HDAC6 expression inversely correlates with HR23B expression in the DLBCL patient sample

Figure S5. MET inhibitor PF-04217903 is not active in DLBCL cells

Figure S6. Ricolinostat in combination with crizotinib produces a synergic effect *in vivo*

Table S1. List of primer sequences used in the NanoString nCounter assays

Table S2. List of antibodies used in this study

Table S3. Correlation between high levels of HDAC6 and HR23B and the clinicopathological characteristics of 151 patients with DLBCL

Table S4. Multivariate Cox proportional hazard analysis of the prognostic variables in DLBCL patients

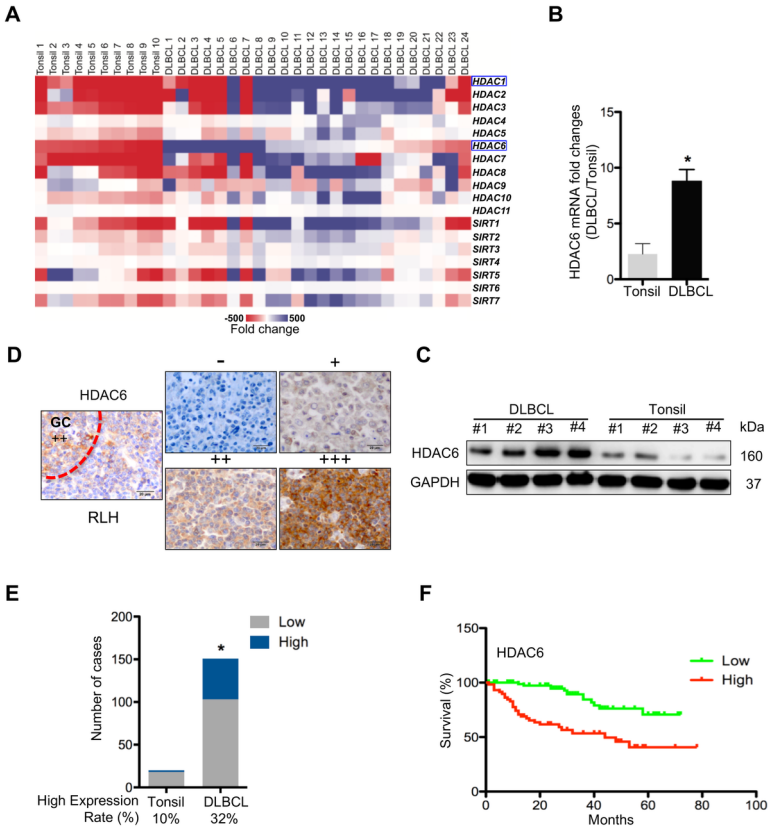

path_5108_fig1.tif

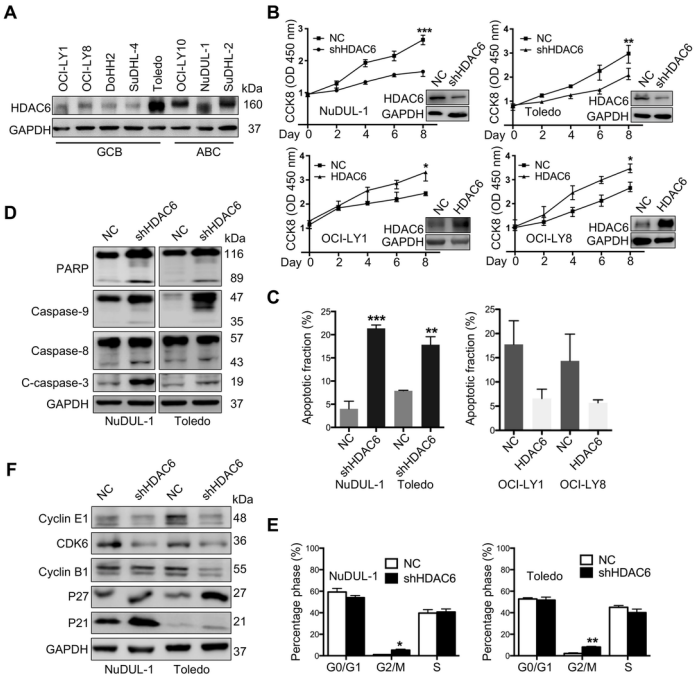

path_5108_fig2.tif

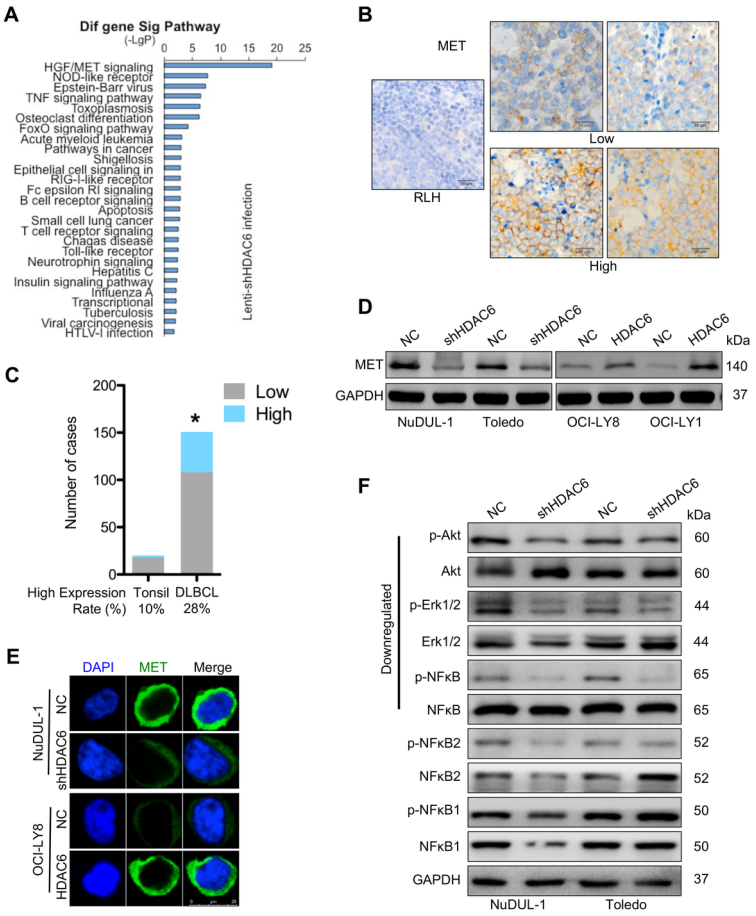

path_5108_fig3.tif

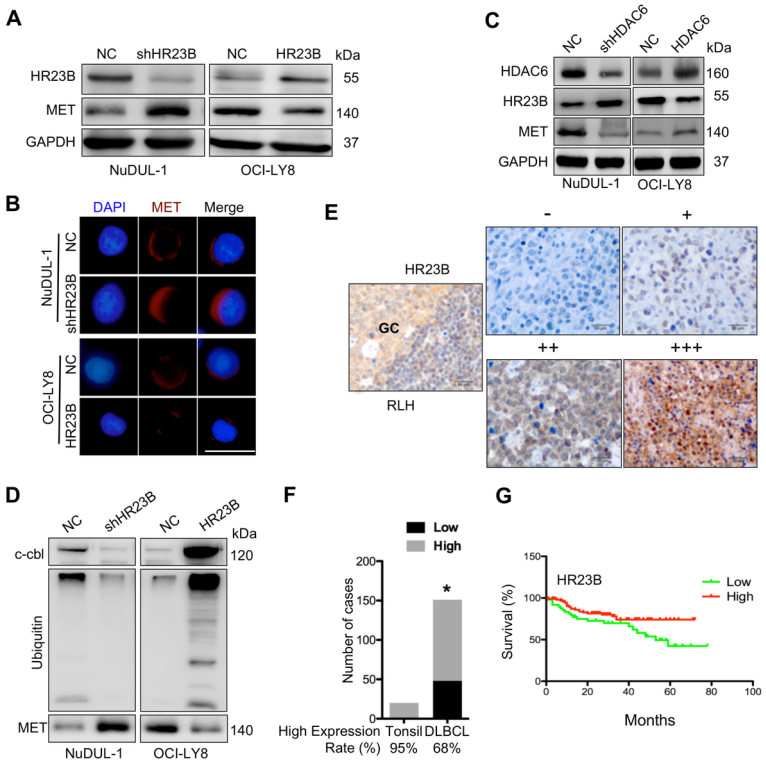

path_5108_fig4.tif

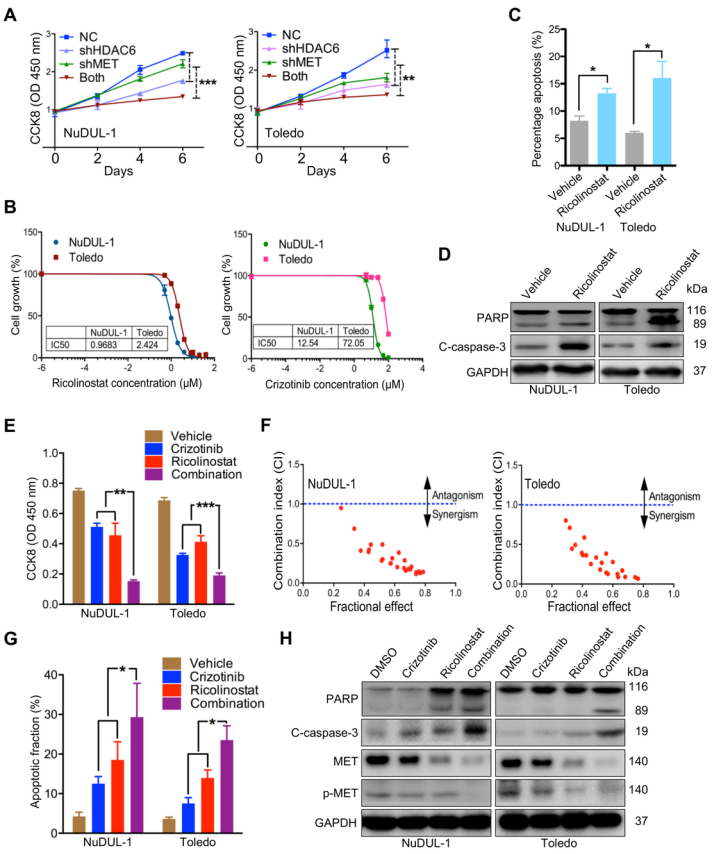

path_5108_fig5.tif

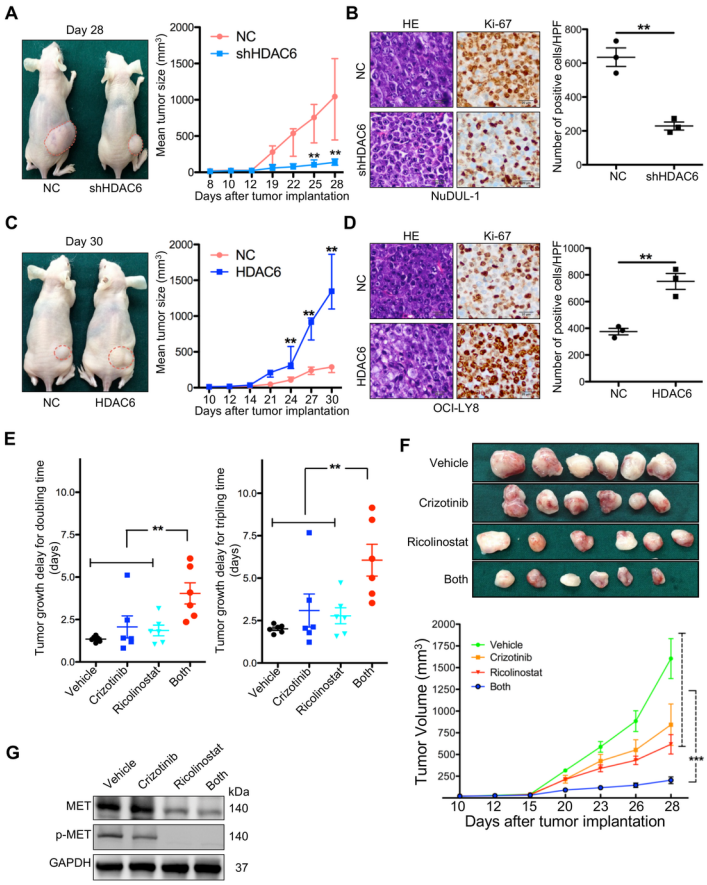

path_5108_fig6.tif

B-1（1.0 版）

复旦大学附属肿瘤医院医学伦理委员会

批准函

伦理编号：050432-4-1212B

审查日期	2012.12.24
审查会议地点	2 号楼 5 楼第五会议室
研究项目名称	组织及外周血样本采集知情同意书
审查文件	相关资料（每单项必须填写，提交资料标记为 ✓，未提交资料的标记为 ╳，如无版本号标记为 — ） ☒ 国家食品药品监督管理局批件，批件文号：_____ ☒ 方案，版本号：_____ ☒ 项目，编号：_____ ☒ 药品生产许可证及检测报告/医疗器械注册证及检验报告 ☑ 知情同意书样本，版本号：复旦大学附属肿瘤医院组织库样本收集知情同意书 2.0 版（2012.12.13） ☒ 研究者履历、临床研究经历 ☒ 其他（请说明）：_____
研究科室	组织库
主要研究者	杜祥
申办者	NA
伦理审查方式	☑会议审查　　□快速审查
投票结果	应到人数：16 人　　实到人数：14 人 回避委员：杜祥（本次会议未出席）
审查意见	同意知情同意书修正。 主任或副主任委员签字： 复旦大学附属肿瘤医院医学伦理委员会（盖章） 日期：2012 年 12 月 24 日

注意：（请仔细阅读）

1. 该研究进行过程中将接受伦理委员会的持续审查，审查频度为研究批准之日起：/（伦理委员会有权根据实际进展情况改变持续审查频度）
2. 本批件将在各中心机构及其伦理委员会备案。
3. 已批准项目须遵循本伦理委员会批准的方案执行，须符合 SFDA/GCP 和《赫尔辛基宣言》的原则。
4. 暂停/提前终止临床研究，请及时通知伦理委员会。
5. 发生严重不良事件及影响研究风险受益比的非预期事件，须及时报告本伦理委员会。
6. 对已批准的临床研究方案、知情同意书等材料的任何修改及主要研究者更换等，须及时通知本伦理委员会重新审查，获得批准后执行。
7. 发现违反方案情况须及时报告伦理委员会。
8. 根据伦理委员会对持续审查频度的意见，无论试验开始与否，请在持续审查日到期前 1 个月提出持续审查的申请。
9. 完成临床研究，须提交结题报告供伦理委员会审查。

附件：伦理委员会签到及保密协议、伦理委员会组成人员名单